第126巻　第12号　平成30年12月１日発行（毎月1回1日発行）　ISSN 1348-6535 CODEN:JCSJEW

JCS-Japan

December

vol.126

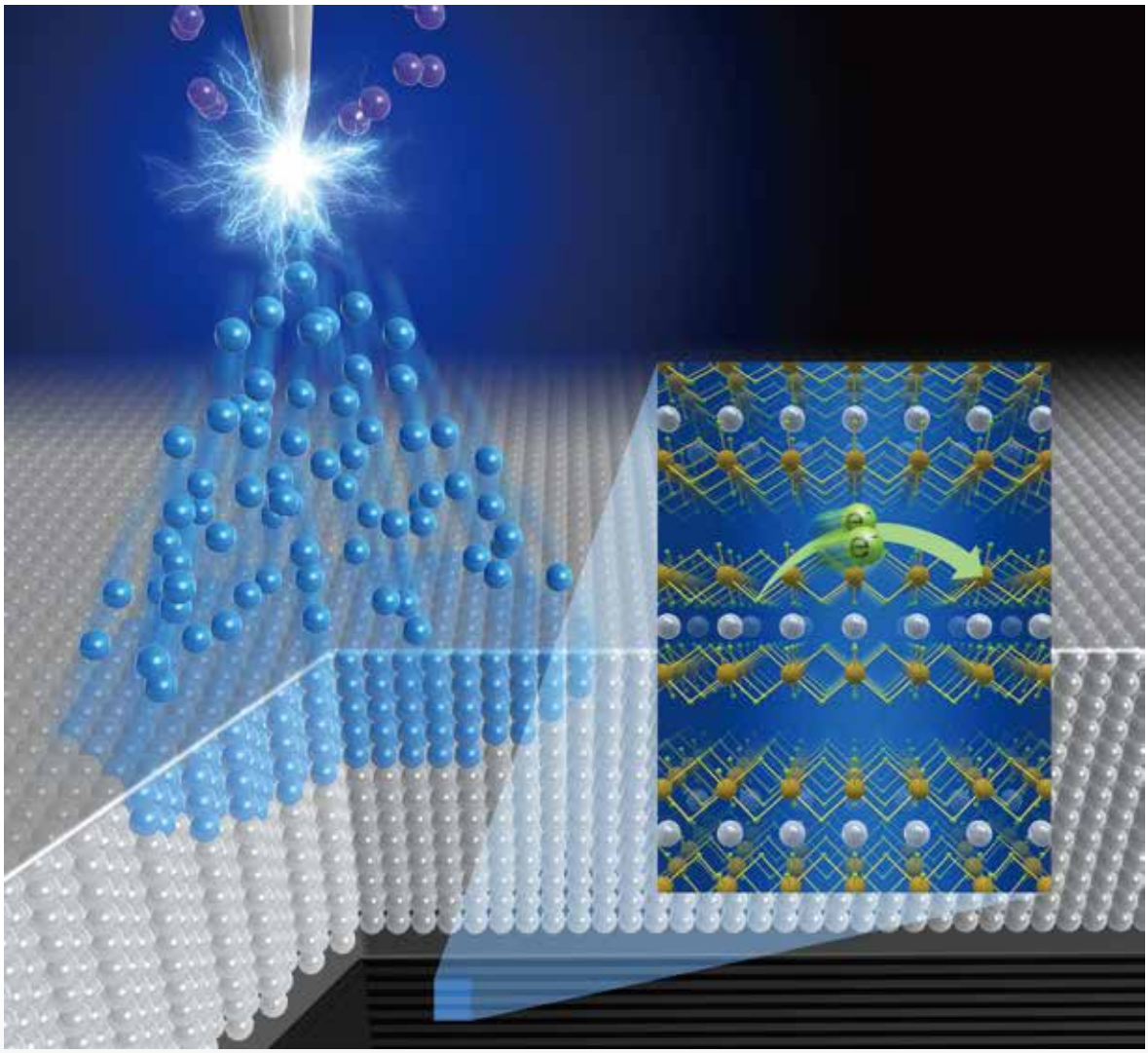

Journal of the Ceramic Society of Japan

2018

Journal of the Ceramic Society of Japan 126 [12] 963-967 2018
DOI http://doi.org/10.2109/jcersj2.18148

JCS-Japan

FULL PAPER

Superconductivity in Ag_xTaS_2 single crystals with stage structure obtained via proton-driven ion introduction

Masaya FUJIOKA[1,†], Naoki KUBO[1], Masanori NAGAO[2], Robin MSISKA[1], Naoki SHIRAKAWA[3], Satoshi DEMURA[4], Hideaki SAKATA[5], Hideo KAIJU[1] and Junji NISHII[1]

[1]Research Institute for Electronic Science, Hokkaido University, N20W10, Kita-Ward Sapporo 001–0020, Japan
[2]Center for Crystal Science and Technology, University of Yamanashi, Kofu 400–8511, Japan
[3]Flexible Electronics Research Center, National Institute of Advanced Industrial Science and Technology (AIST), 1–1–1 Higashi, Tsukuba, Ibaraki 305–8565, Japan
[4]College of Science and Technology, Nihon University, 1–8–14 Surugadai, Kanda, Chiyoda-ku, Tokyo 101–8308, Japan
[5]Graduate school of Science, Tokyo University of Science, 1–3 Kagurazaka, Shinjuku-ku, Tokyo 162–8601, Japan

Ag^+ ions were intercalated into the transition-metal dichalcogenide TaS_2 using the recently developed method of proton-driven ion introduction. Single-crystalline $Ag_{0.58}TaS_2$ with a stage 1 structure and $Ag_{0.21}TaS_2$ with a stage 2 structure were prepared using this method. The stage 2 structure of $Ag_{0.21}TaS_2$ was formed by exploiting the differences in ion diffusion properties among the polytypes of TaS_2. Furthermore, our intercalation method can forcibly insert Ag^+ ions into interlayers by applying a high voltage at low temperature (100°C), resulting in the formation of thermodynamically metastable phase. Such a synthesis approach offers a potential route for diversifying intercalation compounds with different stage structures. The first observations of superconductivity in Ag_xTaS_2 were demonstrated in this study. The onset of superconductivity of Ag_xTaS_2 was estimated to be 0.4 and 1.7 K in the samples with $x = 0.58$ and $x = 0.21$, respectively. Some anomalies, which were speculatively attributed to charge density wave order, were confirmed in the resistivity measurements of Ag_xTaS_2. The results suggested that the anomalies were closely correlated with the superconducting transition temperature.

Key-words : Two-dimensional tantalum disulfide, Intercalation, Superconductivity, Solid state electrochemistry

[Received August 7, 2018; Accepted September 24, 2018]

1. Introduction

Transition-metal dichalcogenides, referred to as MX_2 (M = Ti, Zr, Hf, V, Nb, Ta, Mo, and W; X = S, Se, and Te), are layered structures that exhibit interesting physical properties.[1)–4)] These layered materials are formed by strong in-plane covalent bonding and weak out-of-plane van der Waals interactions. Therefore, various guest species can insert into the interlayers of such structures and form intercalation compounds. TaS_2 is a typical layered transition-metal dichalcogenide that exhibits various polytypes, including the 1T, 2H, 3R, 4Hb, and 6R polytypes.[5)–8)] 2H-TaS_2 easily forms intercalation compounds and also exhibits a coexisting charge density wave (CDW) at 78 K and superconducting transition at 0.8 K.[9)] Its superconductivity is effectively enhanced via the intercalation of various guest species such as organic molecules,[10),11)] alkali metals (Li, Na, and K),[12)–14)] 3d metals (Fe and Cu),[15)–17)] and low-melting metals (Hg, In, Sn, Pb, and Bi).[18)] However, the superconductivity of Ag^+-intercalated TaS_2 has never been reported.

In this study, we prepared Ag_xTaS_2 ($x = 0.58$, 0.21) using the recently developed method of proton-driven ion introduction (PDII)[19)] and demonstrated their superconductivity. **Figure 1**(a) schematizes the PDII process, which is based on a solid-state electrochemical synthesis and achieves high crystallinity and homogeneity of single-crystalline intercalation compounds because of its liquid-free process. The common intercalation methods involving liquid-phase processes result in the simultaneous intercalation of solution molecules and a concentration gradient of guest ions from the surface to the interior of the host material. Therefore, the preparation of intercalated materials with high crystallinity and homogeneously dispersed intercalation species is a substantial challenge. In the PDII process, the protons (H+) generated by the electrolytic dissociation of hydrogen drive other monovalent cations from the top side to the bottom side of a solid electrolyte along a high electric field, as described later. Such a liquid-free process enables us to apply a high voltage on the order of several kilovolts as a driving force for intercalation. Because ion intercalation should be sufficiently filled in the host material to the solid solubility limit to obtain homogeneously intercalated compounds. In our previous report, we synthesized single-crystalline 2H-A_xTaS_2 (A =

† Corresponding author: M. Fujioka; E-mail: fujioka@es.hokudai.ac.jp

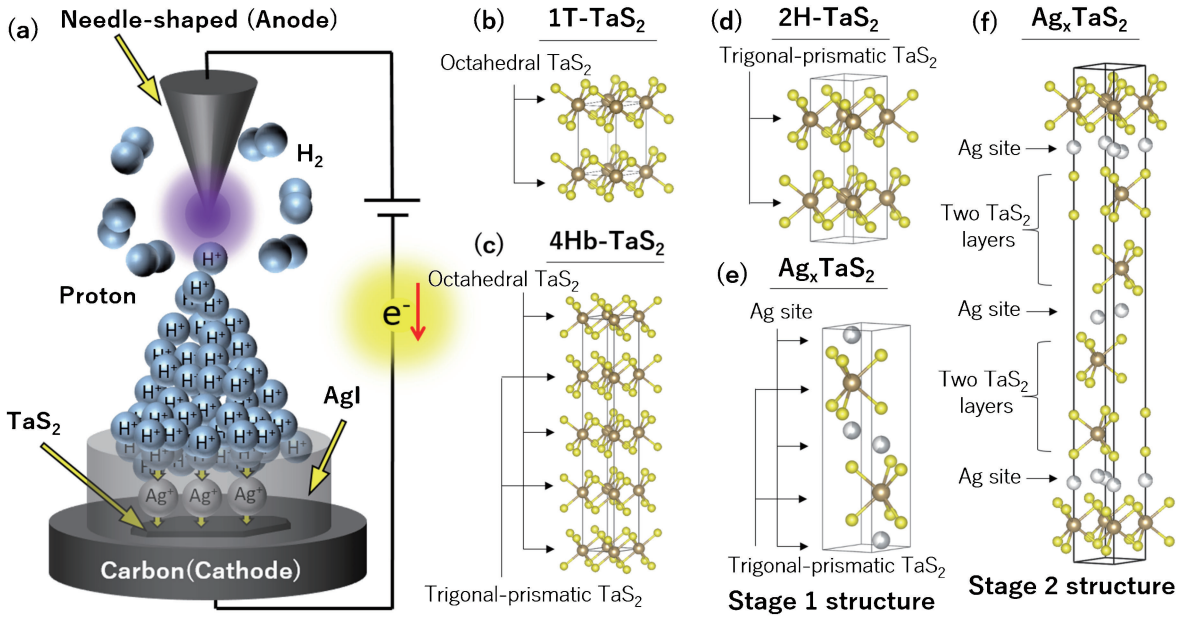

Fig. 1. (a) Schematic of the PDII process. Crystal structures of (b) 1T-TaS_2, (c) 4Hb-TaS_2, (d) 2H-TaS_2, (e) Ag_xTaS_2 with stage 1 structure, and (f) Ag_xTaS_2 with stage 2 structure.

Li, Na, K, Cu, and Ag) while maintaining high homogeneity and crystallinity.[19] These compounds show stage 1 structure as depicted in Fig. 1(e). Guest ions are inserted into every TaS_2 interlayer.

Herein, we synthesized 2H-Ag_xTaS_2 ($x = 0.21$) with a stage 2 structure, as shown in Fig. 1(f), utilizing a polytype of 4Hb-TaS_2 as a host material. Experimentally, guest ions are more difficult to insert into 1T-TaS_2, which is composed of octahedral TaS_2 layers, than into 2H-TaS_2, which is composed of trigonal-prismatic layers [Figs. 1(b) and 1(d)]. Figure 1(c) shows the crystal structure of 4Hb-TaS_2. It has an alternating stacking structure of octahedral (1T) and trigonal-prismatic (2H) TaS_2 layers. Such a crystal structure accommodates Ag+ ions into every other TaS_2 layers, resulting in the formation of a "stage 2" structure.

2. Sample characterization

2.1 Proton-driven ion introduction

To prepare the Ag^+-intercalated TaS_2, single-crystalline 2H- and 4Hb-TaS_2 were grown via chemical vapor transport.[20] Polycrystalline TaS_2 and I_2 (5 mg/cm^3) as a transporting agent were added to a closed quartz tube. They were sintered using a temperature gradient from 800 to 900°C for seven days. Plate-like single crystals, including 2H- and 4Hb-TaS_2, were obtained. Figure 1(a) schematizes the PDII process. To intercalate Ag^+ ions into the single-crystalline 2H- and 4Hb-TaS_2, AgI was adopted as an appropriate ion source of solid electrolyte because of its high Ag^+-ion conductivity.[21] Thus, pelletized AgI was placed on the single-crystalline TaS_2 under a 100% H_2 atmosphere. When a high voltage is applied between the needle-shaped anode and the carbon cathode, protons are generated and accelerated to the pelletized AgI along the electric field. They then penetrate and push the Ag^+ ions from the top side to the bottom side. Because charge neutrality should be retained in the AgI, the Ag^+ ions must be released from the bottom side and intercalated into TaS_2. Simultaneously, TaS_2 receives electrons form the carbon cathode. Thus, the reaction of $TaS_2 + xA^+ + xe^- \rightleftharpoons A_xTaS_2$ is driven.

Our previous study on PDII revealed that the ion supply rate from the ion source should be smaller than the ion diffusion rate of the host material; otherwise, surplus Ag^+ is precipitated as Ag metal at the interface between AgI and TaS_2. Such a precipitation separates them and prevents Ag^+ from migrating to the TaS_2. The ion supply rate, which corresponds to the electric current flowing around the circuit, and the ion diffusion rate can be controlled by adjusting the applied voltage and the treatment temperature, respectively.

2.2 $Ag_{0.58}TaS_2$ with stage 1 structure

2H-TaS_2 was treated with PDII, wherein 1.8 kV of voltage was applied between electrodes at 400°C. The electric current was then increased to 11 μA. Under this treatment condition, homogeneous 2H-Ag_xTaS_2 with stage 1 was obtained. The chemical composition was estimated to be $Ag_{0.58}Ta_{1.00}S_{1.95}$ by using inductively coupled plasma mass spectrometry (ICP). In addition, the high crystallinity of the sample was confirmed via X-ray diffraction (XRD) measurements using Cu Kα radiation, as shown in **Fig. 2**(a). Observed full width of half maximum (FWHM) of the main peaks are almost comparable between pristine TaS_2 and $Ag_{0.58}TaS_2$. Also, the (00l)- indexed peaks in the XRD pattern shifted to lower angles, and the c lattice parameter is expanded from 12.08 to 14.46 Å after Ag intercalation. The basal spacing of $Ag_{0.58}TaS_2$ is 7.23 Å.

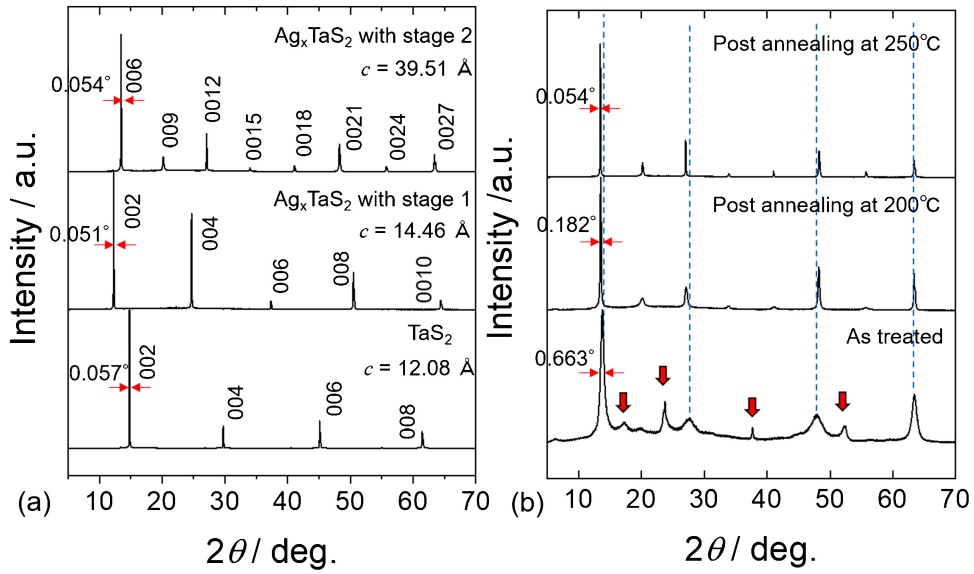

Fig. 2. (a) XRD patterns for pristine TaS_2 and Ag^+ intercalated TaS_2 with stage 1 and 2 structures. (b) Post annealing temperature dependence of normalized XRD patterns for Ag^+-intercalated 4Hb-TaS_2.

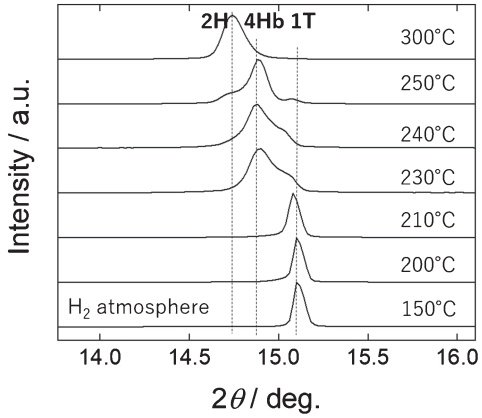

Fig. 3. Shift of the (002) XRD peak of 1T-TaS_2 after post annealing at various temperatures under a H_2 atmosphere. 1T-TaS_2 gradually transforms to 2H-TaS_2 via 4Hb-TaS_2.

2.3 $Ag_{0.21}TaS_2$ with stage 2 structure

As described above, polytype single-crystalline 4Hb-TaS_2 was used as a host material to obtain a stage 2 structured Ag_xTaS_2. However, at a high temperature such as 400°C and under a H_2 atmosphere, the 4Hb structure changes to 2H (**Fig. 3**). Therefore, the treatment temperature was kept at 100°C to maintain the 4Hb structure during PDII. We adjusted the voltage to satisfy the aforementioned relation; specifically, the ion supply rate was maintained lower than ion diffusion rate at 100°C. Under an applied voltage of 3.0 kV, 5–6 μA of electric current flowed around the circuit. Note that a higher voltage is necessary for ion migration across the PDII cell under a lower temperature, because of the decrease in the ion diffusion coefficient of the ion source.

In Fig. 2(b), as treated single crystal by PDII showed broad XRD peaks. However, as described FWHM, some peaks narrowed after the crystal was annealed at 200 and 250°C, and the other peaks (indicated by red arrows) disappeared. Even when the annealing temperature was increased to 300°C, the obtained XRD results were comparable with those at 250°C. Furthermore, each peak indexed as (00l) shifts to a lower or higher angle as annealing temperature is increased. Blue-dotted lines are added for clarity. These results suggest that the post annealing does not simply improve the crystallinity of Ag^+-intercalated TaS_2 but induces a structural stabilization through the transformation from octahedral to trigonal-prismatic TaS_2. In fact, Fig. 3 shows that the thermal treatment at around 300°C transforms the 4Hb structure into a 2H structure. The same transformation is expected to be induced. Specifically, the Ag^+-intercalated 4Hb structure changed to the 2H structure during post-annealing. This irreversible phase transition means that the as treated material by PDII shows the thermodynamically metastable phase. This is because the guest ions are forcibly intercalated into interlayers by applying a high voltage at low temperature. Although the detailed crystal structure of Ag^+-intercalated 4Hb-TaS_2 is difficult to determine from the current XRD results as shown in Fig. 2(b), these findings demonstrate that the PDII is one of the most promising methods to synthesizes unobtainable materials by traditional solid-state reaction.

As shown in Fig. 2(a), peak-to-peak intervals in Ag_xTaS_2 obtained from 4Hb structure are reduced by almost half in comparison with $Ag_{0.58}TaS_2$. This means that the c lattice constant significantly increases. On the other hand, from the ICP measurement, the chemical composition was estimated to be $Ag_{0.21}Ta_{1.00}S_{1.90}$. The amount of Ag is less than half of stage 1 structured $Ag_{0.58}TaS_2$. These results strongly support the formation of a multi-stage structure in $Ag_{0.21}TaS_2$. Actually, XRD peak positions of $Ag_{0.21}TaS_2$ agree well with the (00l) indexed peak positions obtained from previously reported XRD patterns

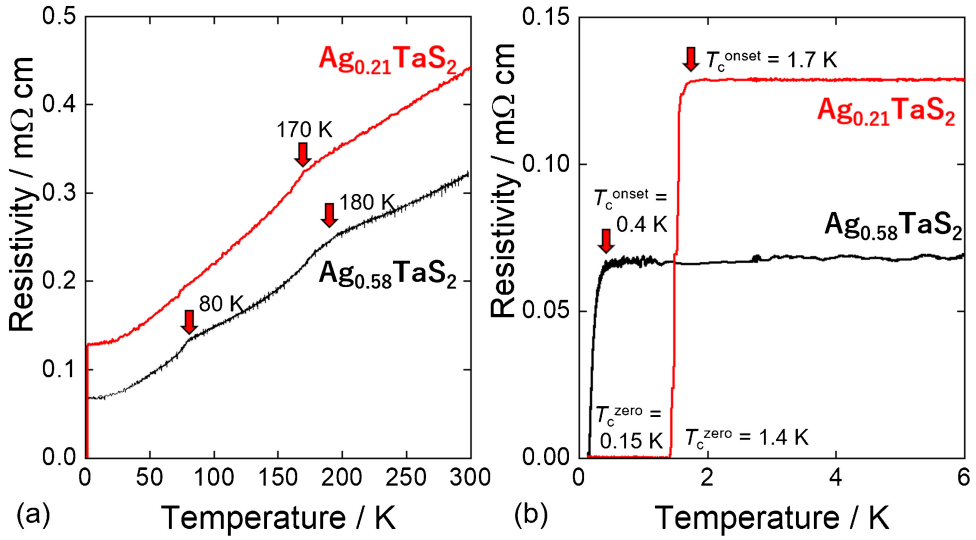

Fig. 4. (a) Temperature dependence of the resistivity for $Ag_{0.58}TaS_2$ and $Ag_{0.21}TaS_2$ from 0.15 to 300 K. (b) An expanded view of (a).

of powdered Ag_xTaS_2 with stage 2 structure.[22] From these results, we concluded that the stage 2 structure should be formed in $Ag_{0.21}TaS_2$. However, accurate analysis is necessary to discuss the detailed crystal structure of $Ag_{0.21}TaS_2$. In the current stage, only the c lattice parameter of $Ag_{0.21}TaS_2$ (39.51 Å) can be estimated. The basal spacing of $Ag_{0.21}TaS_2$ is 13.17 Å. Since this basal spacing includes two TaS_2 layers, it is much larger than that of $Ag_{0.58}TaS_2$ (7.23 Å).

3. Experimental results and discussion

3.1 Electric measurements of Ag_xTaS_2

Electrical resistivity was measured by a standard four-probe method from 300 to 0.13 K using an adiabatic demagnetization refrigerator system [Quantum Design, Physical Property Measurement System]. The single-crystalline Ag_xTaS_2 ($x = 0.21$ and 0.58) samples were formed into rectangles with dimensions of approximately $2.17 \times 0.58 \times 0.03\ mm^3$ and $2.03 \times 0.92 \times 0.04\ mm^3$, respectively. **Figure 4** shows the temperature dependence of resistivity for the samples with $x = 0.21$ and 0.58. The resistivity gradually decreases with decreasing temperature, thereby indicating metallic behavior. Finally, superconductivity appeared at $T_c^{onset} = 0.4$ K and $T_c^{zero} = 0.15$ K on the black line denoting $x = 0.58$ and at $T_c^{onset} = 1.7$ K and $T_c^{zero} = 1.4$ K on the red line denoting $x = 0.21$. In this study, T_c^{onset} was regarded as the starting point of the decrease in resistivity from the normal conducting state and T_c^{zero} was regarded as the point at which the line for zero resistivity crossed the ρ–T curve.

3.2 Magnetic measurements of $Ag_{0.21}TaS_2$

Superconducting transition was also observed from magnetic measurements using a superconducting quantum device magnetometer [Quantum Design, Magnetic Property Measurement System].[23] **Figure 5** shows the temperature dependence of the field-cooled (FC) and zero-field-cooled (ZFC) susceptibility of $Ag_{0.21}TaS_2$ from 0.47 to 1.9 K under a 10 Oe field. To reduce the demagnetizing effect, a magnetic field was applied parallel to the ab plane of the single crystal. Although the obtained signal is noisy because of the small sample, the FC and ZFC curves separate at approximately 1.2 K and the superconducting volume fraction is estimated to be almost 100% at 0.5 K. Therefore, the bulk superconductivity of $Ag_{0.21}TaS_2$ is confirmed. Because the T_c of $Ag_{0.58}TaS5_2$ is lower than the lowest achievable temperature, the Meissner effect of $Ag_{0.58}TaS_2$ could not be detected. However, since the XRD and EDS measurements provide supporting evidence that the obtained samples were single phase, the observed superconductivity at 0.4 K should be the nature of $Ag_{0.58}TaS_2$.

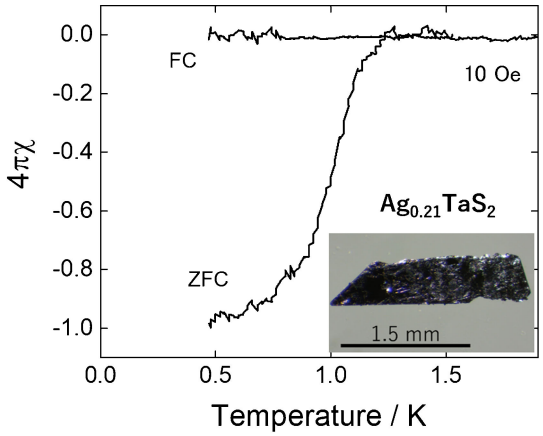

Fig. 5. Temperature dependence of magnetic susceptibility for $Ag_{0.21}TaS_2$ under a 10 Oe field. The inset image is a photograph of the single-crystalline $Ag_{0.21}TaS_2$.

3.3 Relationship between T_c and CDW

As shown in Fig. 4(a), two anomalies are observed at 180 and 80 K in the ρ–T curve of $Ag_{0.58}TaS_2$. An anomaly

was also observed in $Ag_{0.21}TaS_2$ at a similar temperature of ~170 K; however, the anomaly observed at 80 K in the curve for $Ag_{0.58}TaS_2$ was not observed in the curve of $Ag_{0.21}TaS_2$. Because the host material of 2H-TaS_2 shows a CDW at 78 K, these anomalies are also considered to be caused by CDWs.[9] In addition, the suppressed CDW is widely acknowledged to lead to an increase in the density of states at the Fermi level and to ultimately enhance T_c according to McMillan's theory.[24] This concept qualitatively explains the resistivity behavior of these Ag_xTaS_2 ($x = 0$, 0.21, 0.58) compounds. When the Ag^+ concentration decreased from $x = 0.58$ to $x = 0.21$, the CDW at 80 K in $Ag_{0.58}TaS_2$ was suppressed and the T_c increased from 0.4 to 1.7 K. Likewise, a comparison of the samples with $x = 0.58$ and $x = 0$ suggests that the suppressed CDW at 180 K enhances T_c from 0.4 K ($x = 0.58$) to 0.8 K ($x = 0$). Although the origin of anomalies must be clarified using transmission electron microscopy and scanning tunneling microscopy, the results for Ag_xTaS_2 ($x = 0$, 0.21, 0.58) are in good agreement with the known relationship between CDW and superconductivity.[24]

4. Conclusion

We have successfully synthesized single-crystalline Ag_xTaS_2 ($x = 0.58$, 0.21) via PDII. The synthetic route to Ag_xTaS_2 with the stage 2 structure exploited the difference in ion diffusion rates among the polytypes of octahedral and trigonal-prismatic layers. Ag^+ ions were forcibly inserted into interlayers of 4Hb-TaS_2 by PDII at 100°C, resulting in the formation of a thermodynamically metastable phase. This approach has potential applications for diversifying intercalation compounds since such stage structures are expected to provide previously unknown physical properties. In fact, Ag_xTaS_2 exhibited the onset of superconductivity at 0.4 and 1.7 K for $x = 0.58$ and 0.21, respectively. Some anomalies observed in the resistivity measurements at higher temperatures seem to correlate with the superconducting T_c's and are speculatively attributed to CDW order.

Acknowledgements This research has been partially supported by a Grant-in-Aid for Challenging Exploratory Research from the Japan Society for the Promotion of Science (JSPS; Grant No. 17K19166 and 18K19122), Iketani Science and Technology Foundation, Nanotech Career-up Alliance (CUPAL), Environment and Materials and the Cooperative Research Program of the Network Joint Research Center for Materials and Devices from the Ministry of Education, Culture, Sports, Science and Technology (MEXT).

Reference

1) W. Choi, N. Choudhary, G. H. Han, J. Park, D. Akinwande and Y. H. Lee, *Mater. Today*, **20**, 116–130 (2017).
2) M. Zhang, Y. Zhu, X. Wang, Q. Feng, S. Qiao, W. Wen, Y. Chen, M. Cui, J. Zhang, C. Cai and L. Xie, *J. Am. Chem. Soc.*, **137**, 7051–7054 (2015).
3) K. Xu, Z. Wang, F. Wang, Y. Huang, F. Wang, L. Yin, C. Jiang and J. He, *Adv. Mater.*, **27**, 7881–7887 (2015).
4) E. Navarro-Moratalla, J. O. Island, S. Mañas-Valero, E. Pinilla-Cienfuegos, A. Castellanos-Gomez, J. Quereda, G. Rubio-Bollinger, L. Chirolli, J. A. Silva-Guillén, N. Agraït, G. A. Steele, F. Guinea, H. S. J. van der Zant and E. Coronado, *Nat. Commun.*, **7**, 11043 (2016).
5) B. Sipos, A. F. Kusmartseva, A. Akrap, H. Berger, L. Forr and E. Tutis, *Nat. Mater.*, **7**, 960–965 (2008).
6) S. F. Meyer, R. E. Howard, G. R. Stewart, J. V. Acrivos and T. H. Geballe, *J. Chem. Phys.*, **62**, 4411–4419 (1975).
7) A. H. Thompson, *Solid State Commun.*, **17**, 1115–1117 (1975).
8) Y. Feng, S. Gong, E. Du, X. Chen, R. Qi, K. Yu and Z. Zhu, *J. Phys. Chem. C*, **122**, 2382–2390 (2018).
9) J. M. E. Harper, T. H. Geballe and F. J. DiSalvo, *Phys. Rev. B*, **15**, 2943–2951 (1977).
10) F. R. Gamble, F. J. DiSalvo, R. A. Klemm and T. H. Geballe, *Science*, **168**, 568–570 (1970).
11) G. V. S. Rao, M. W. Shafer and J. C. Tsang, *J. Phys. Chem.*, **79**, 553–557 (1975).
12) F. Sernetz, A. Lerf and R. Schöllhorn, *Mater. Res. Bull.*, **9**, 1597–1602 (1974).
13) L. Fang, P. Y. Zou, Y. Wang, L. Tang, Z. Xu, H. Chen, C. Dong, L. Shan and H. H. Wen, *Sci. Technol. Adv. Mater.*, **6**, 736–739 (2005).
14) A. Lerf, F. Sernetz, W. Biberacher and R. Schöllhorn, *Mater. Res. Bull.*, **14**, 797–805 (1979).
15) K. E. Wagner, E. Morosan, Y. S. Hor, J. Tao, Y. Zhu, T. Sanders, T. M. McQueen, H. W. Zandbergen, A. J. Williams, D. V. West and R. J. Cava, *Phys. Rev. B*, **78**, 104520 (2008).
16) X. Zhu, Y. Sun, S. Zhang, J. Wang, L. Zou, L. E. DeLong, X. Zhu, X. Luo, B. Wang, G. Li, Z. Yang and W. Song, *J. Phys.-Condens. Mat.*, **21**, 145701 (2009).
17) R. M. Fleming and R. V. Coleman, *Phys. Rev. Lett.*, **34**, 1502–1505 (1975).
18) F. J. Di Salvo, G. W. Hull, Jr., L. H. Schwartz, J. M. Voorhoeve and J. V. Waszczak, *J. Chem. Phys.*, **59**, 1922–1929 (1973).
19) M. Fujioka, C. Wu, N. Kubo, G. Zhao, A. Inoishi, S. Okada, S. Demura, H. Sakata, M. Ishimaru, H. Kaiju and J. Nishii, *J. Am. Chem. Soc.*, **139**, 17987 (2017).
20) A. Ubaldini and E. Giannini, *J. Cryst. Growth*, **401**, 878–882 (2014).
21) D. A. Keen, S. Hull, A. C. Barnes, P. Berastegui, W. A. Crichton, P. A. Madden, M. G. Tucker and M. Wilson, *Phys. Rev. B*, **68**, 014117 (2003).
22) J. Mahy, G. A. Wiegers, F. van Bolhuis, A. Diedering and R. J. Haange, *Phys. Status Solidi A*, **107**, 873–887 (1988).
23) N. Shirakawa and M. Tamura, *Polyhedron*, **24**, 2405–2408 (2005).
24) A. M. Gabovicha, A. I. Voitenkoa and M. Ausloosb, *Phys. Rep.*, **367**, 583–709 (2002).